

This version has been accepted for publication after peer review, but does not include post-acceptance corrections and formatting improvements. The version of records can be found on the publisher's digital library entry: doi.org/10.1016/j.heares.2025.109320.

©2025. Manuscript made available under the CC-BY-NC-ND 4.0 license
creativecommons.org/licenses/by-nc-nd/4.0/

Active control of transverse viscoelastic damping in the tectorial membrane: a second mechanism for traveling-wave amplification?

François Deloche^a, Morgan Thienpont^a, Arturo Moleti^b, Renata Sisto^c, Sarah Verhulst^a

^aHearing Technology @WAVES, Department of Information Technology, Ghent University, Ghent, Belgium

^bDepartment of Physics, University of Rome Tor Vergata, Rome, Italy

^cDepartment of Occupational and Environmental Medicine, Epidemiology and Hygiene, Italian Workers Compensation Authority, Monte Porzio Catone (Rome), Italy

Abstract

Observations from optical coherence tomography (OCT) have revealed a velocity gradient across the reticular lamina in response to sounds [Cho and Puria, *Scientific Reports*, **12**, 18715 (2022)]. Since viscoelastic forces depend on velocity gradients, this finding suggests that OHC activity may influence viscous loss in the cochlea. Here, we propose a candidate mechanism for regulating traveling-wave viscous dissipation which involves the tectorial membrane (TM). We hypothesize that the velocity gradient generated in the OHC region, combined with TM structural properties, can reduce transverse deformations in the TM and, subsequently, transverse viscous damping. Based on this hypothesis and a simplified mechanical model, we derive a formula for an equivalent basilar membrane (BM) admittance in both passive and active scenarios. We use the WKB approximation to simulate traveling waves in response to tones at different stimulation levels. The calibration of the model is based on OCT data from mice, including data on TM motion. Our simulations show that modulating the viscous load affects the traveling wave in the peak region, with changes in BM velocity magnitude of up to 10 dB. The inclusion of a more classical anti-damping term is necessary to capture the full dynamic range of the response gain. With the textbook view of OHCs acting directly on the BM under re-evaluation in light of recent OCT data, the control of viscous damping in the TM emerges as a viable candidate for a second mechanism governing traveling-wave amplification.

Keywords: cochlear mechanics, traveling wave, outer hair cells, tectorial membrane, viscosity

1. Introduction

In the healthy mammalian cochlea, vibrations evoked by tones exhibit characteristics that vary with sound intensity level. At behavior thresholds, the gain of basilar membrane (BM) displacement at the characteristic place is at least 30 dB higher than for high stimulus intensities [1, 2, 3, 4, 5, 6]. This gain decrease has alternately been interpreted as indicative of the amplification of low-intensity traveling waves (e.g, [5, 7]), or as evidence of the compression of higher-intensity waves [8]. The exact mechanisms involved in this nonlinear process —

also called the “active process” of the cochlea — are partly unknown or still under debate, although it is widely accepted that the electromotile outer hair cells (OHCs) play a critical role [7, 9, 10, 11]. A commonly cited mechanism underpinning the active process is the push-pull action of OHCs. This mechanism suggests that the cell bodies of the OHCs contract when the BM goes up, in response to well-timed hair cell deflections caused by shear motion between the tectorial membrane (TM) and the reticular lamina (RL). As a result, OHCs would exert a pulling force on the basilar membrane (BM), amplifying its upward motion [10, 12]. However, recent experimental data, including observations from optical coherence tomography (OCT), have revealed unexpected motion patterns in the organ of Corti, with movement in the OHC region showing more independence from BM motion than previously generally assumed [2, 4, 13]. OCT data has also raised questions about the timing of the OHCs to operate at the correct phase [14, 15], since new measurements indicate a slight phase lead of the RL over BM at frequencies below the characteristic frequency [16, 17], rather than the quarter-cycle phase lag predicted by the push-pull hypothesis [15]. These patterns appear at odds with the apparent simplicity of the push-pull action of OHCs, leaving room for alternative, less direct explanations of the active process [14, 15].

This paper introduces the hypothesis of an additional role for OHCs in controlling transverse viscoelastic damping occurring in the TM. The existence of a ‘friction control’ mechanism capable of modulating cochlear gain has already been proposed by some authors [8, 18]. The hypothesis presented here, however, originates from two other recent studies. The first is a modeling study that described the opposing roles of two hydrodynamic effects — ‘fluid focusing’ and fluid viscous dissipation — on the traveling wave [19, 20]. Both effects are wavelength-dependent and increase in strength in the short-wave region, where the traveling wave in response to a tone reaches its peak amplitude. This work highlighted the potential role of viscosity in stabilizing cochlear amplification and provided a simple mathematical framework to include viscous dissipation in simulations of cochlear pressure waves using the WKB approximation. The second study is a report of OCT data showing the existence of a velocity gradient in the OHC region during auditory stimulation in live gerbils [16]. The authors showed that the part of the RL above the innermost row of OHCs moved with lower amplitude than for the two other rows by a factor of about 10 dB. This observation was valid on a wide range of frequencies around the characteristic frequency (CF).

Our premise is that the radial gradient of transverse velocity observed in the OHC region can modulate transverse deformation in the TM, thus affecting viscoelastic loss in the TM mechanically coupled to the organ of Corti and BM. In this paper, we explore the implications of this hypothesis through a formal analysis carried out under simplifying assumptions, followed by numerical simulations of tone-evoked cochlear waves using the WKB method. Our approach focuses on the traveling wave, assuming that its critical element is the BM moving transversely. In particular, the complex interplay between the active process, TM (radial) load, and hair cell deflection, is beyond the scope of this study. This simplified modeling approach allows us to present an overview of important ideas related to the proposed viscous undamping mechanism, without addressing all the micromechanical or biophysical details of how it could



be implemented in the cochlea.

2. Methods

2.1. Proposed mechanism

To limit the description of the proposed mechanism to its core ideas, we make several simplifying assumptions. We consider that the TM is a nearly incompressible material (Poisson ratio close to 0.5), allowing viscous stresses to be expressed as:

$$\boldsymbol{\tau} = \mu_{TM} [\nabla \mathbf{v} + (\nabla \mathbf{v})^T], \quad (1)$$

where μ_{TM} represents the dynamic viscosity of the TM and $\nabla \mathbf{v}$ is the gradient of velocity. We only consider the transverse components of the velocities — and the transverse derivatives of the (transverse) velocities for the gradients. Radial variations are ignored, except in the next subsection on the analysis of deformation modes. We further assume that the TM has a rectangular shape with the lower and upper surfaces parallel to the BM (i.e., orthogonal to the transverse direction).

Figure 1 shows a schematic of the hypothesized velocity gradients and associated viscous forces at play. Note that in this initial modeling approach, we omit any consideration of phase. We assume that the RL above the OHCs and the TM move in phase with the BM. This is a simplification, as a phase shift of the RL relative to the BM is observed in the best frequency region [16]. The passive and active scenarios are described below.

1) *Passive case* (Fig. 1 left): In 2-D box models of the cochlea, the fluid velocity decays exponentially in the short-wave region with respect to the distance from the BM [10, 20]. In absence of OHC activity, we assume that the velocity in the TM follows the same decreasing trend. When the BM moves up, this results in a gradient of velocity $\nabla \mathbf{v}$ directed toward the BM (negative gradient). To simplify, we consider that the motion is characterized by an irrotational flow, so that the the viscous stress tensor has zero divergence within the TM. In this case, there is no contribution of viscous forces in the bulk of the TM, but the TM is still subject to two normal viscous forces acting on its lower and upper surfaces, equal to:

$$2\mu_{TM} S_{TM} \nabla \mathbf{v} \cdot \vec{n}. \quad (2)$$

S_{TM} is the area of the lower/upper surface for the longitudinal section under consideration, and \vec{n} is a unitary vector normal to the surface pointing in the direction of the TM body. We neglect the viscous contribution from the scala media fluid as the TM viscosity constant is two orders of magnitude higher than that of water [21]. On the lower surface, the viscous stress gives rise to a damping force $2\mu_{TM} S_{TM} \nabla v$ opposing BM velocity (v_{BM}). Conversely, on the upper surface, it generates an anti-damping force equal to $-2\mu_{TM} S_{TM} \nabla v$. However, as motion decays with the distance from the BM, this second force is of lower magnitude than the first one, resulting in a net damping effect.



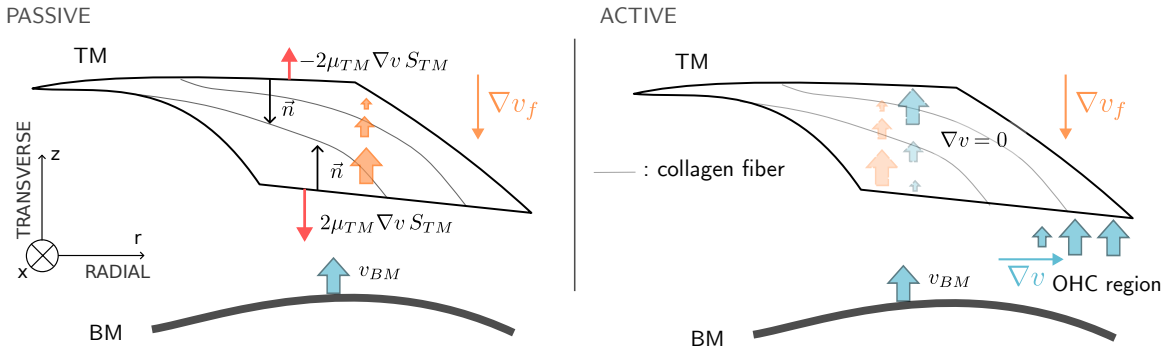


Figure 1: Diagram of hypothesized transverse velocity vectors (thick arrows), velocity gradients (thin blue and orange arrows) and viscous forces (red arrows) associated with an upward motion of the BM, shown on a simplified cross-section view of the cochlea. The TM is depicted as a rhombus for visualization, but is further simplified to a rectangular shape in the main text. **Left:** In the passive case, a velocity gradient pointing downwards generates opposing viscous forces on the lower and upper surfaces on the TM, resulting in net viscous damping. **Right:** In the active case, the reduction of transverse viscous loss would result from the cancellation of the transverse velocity gradient within the TM. This would be the consequence of the velocity gradient observed in the OHC region (blue arrows) opposing the velocity gradient present in the passive state (orange arrows).

2) *Active case* (Fig. 1 right): when the OHCs are active, we assume that the gradient of transverse velocity observed across the RL, mechanically coupled to the TM via the OHC hair bundles, can interfere with the velocity field described in the passive case. To describe the result of this interference, it is helpful to represent the total velocity field as the sum of two components — even though they may not be separable in reality — represented by the faded blue and orange arrows on the diagram. The arrows correspond to two velocity fields that have opposite contributions to the velocity gradient: one is the same as in the passive case (orange arrows, positive velocity gradient), and the other is induced by the motion across the RL (blue arrows, negative velocity gradient). Our assumption is that the sum of these two velocity fields cancels the transverse velocity gradient within the TM, thereby suppressing the normal viscous forces present in the passive case.

However, one may notice an inconsistency in this reasoning: we assume that the OHCs have an effect on the transverse gradient of (transverse) velocity, while observations in the OHC region demonstrate a radial — not transverse — gradient of (transverse) velocity. This apparent discrepancy could be explained by the arrangement of radially-oriented collagen fibers within the TM, which exhibit a downward inclination [22, 23] or even a more pronounced turn towards the BM approaching the marginal zone [24]. Since the collagen fibers provide more mechanical support compared to the softer gel-like matrix of the TM, the role of this configuration may be to reorient the velocity gradient induced by motion across the RL from the radial to the transverse direction. To illustrate this idea, let us consider a scenario where the only source of TM motion is the OHCs attached to the TM marginal zone. If we assume that the velocity

is uniform along each collagen fiber, the resulting velocity gradient stays perpendicular to the fibers. In the marginal zone, this gradient is primarily radial, but as we move towards the limbal region, it gradually shifts to a more transverse direction. Note that this explanation makes the proposed mechanism internally consistent, but we did not test the underlying assumptions experimentally or through additional modeling; hence, at this stage, the proposed mechanism should only be regarded as a formal hypothesis.

2.2. Deformation modes in the TM

Several implications of the proposed mechanism can be inferred by trying to characterize the motion of the TM in the passive and active scenarios. To carry out the analysis, a few more assumptions are made. We consider that the TM impedance is dominated by mass and viscosity at frequencies near CF in the marginal region. We consider that the flow in the TM is incompressible and irrotational, and can be expressed with the gradient of a pressure field satisfying Laplace's equation. We further assume that in a cross-section of the cochlea, the pressure p in response to a tone satisfies the same equation as the fluid above the BM in a 3-D box model (p is in its complex version):

$$\Delta p = k^2 p, \quad (3)$$

where Δ is the 2-D Laplacian, and k is the complex wavenumber. This equation assumes the existence of a longitudinal compression wave in the TM: the relevance of this assumption is discussed at the end of the paper. Solving this equation is difficult because it depends on the geometry of the TM and on the pressure or velocity field in the surrounding fluid. However, we can gain some insight from the following tentative approximation:

$$p_1(r, z) \propto \exp(-k_z z) \exp(-k_r r). \quad (4)$$

In this formula, the decrease along the transverse direction mirrors the exponential decay of fluid pressure above the BM in the short-wave region. The exponential factors for both the radial and transverse directions have negative arguments, consistent with the radial motion of the TM being outward as the BM moves upward [3]. The derivation of the vector field based on this approximation can however only hold in the marginal region of the TM, as the increasing Young's modulus near the limbus [25, 26] restricts motion in that region.

Equation 4 is a solution to Laplace's equation (Eq. 3) when $k_z^2 + k_r^2 = k^2$. In the passive case, we assume that $k_z = k_r = k/\sqrt{2}$. This corresponds to the hypothesis that radial and transverse deformations have equal magnitude, which holds if any factor of anisotropy is disregarded. A second argument is the observation that radial and transverse velocity in the TM, related to the first derivatives of the pressure field, are almost identical in magnitude in the short-wave region at high sound levels (Fig. 2C, OCT vibration data in mice). Eq. 4 will be useful to derive an expression for the viscous stress acting on the TM in the passive mode.

In the active case, our hypothesis suggests that the transverse deformation of the TM is suppressed. Therefore, we introduce a second mode of motion characterized by the absence of



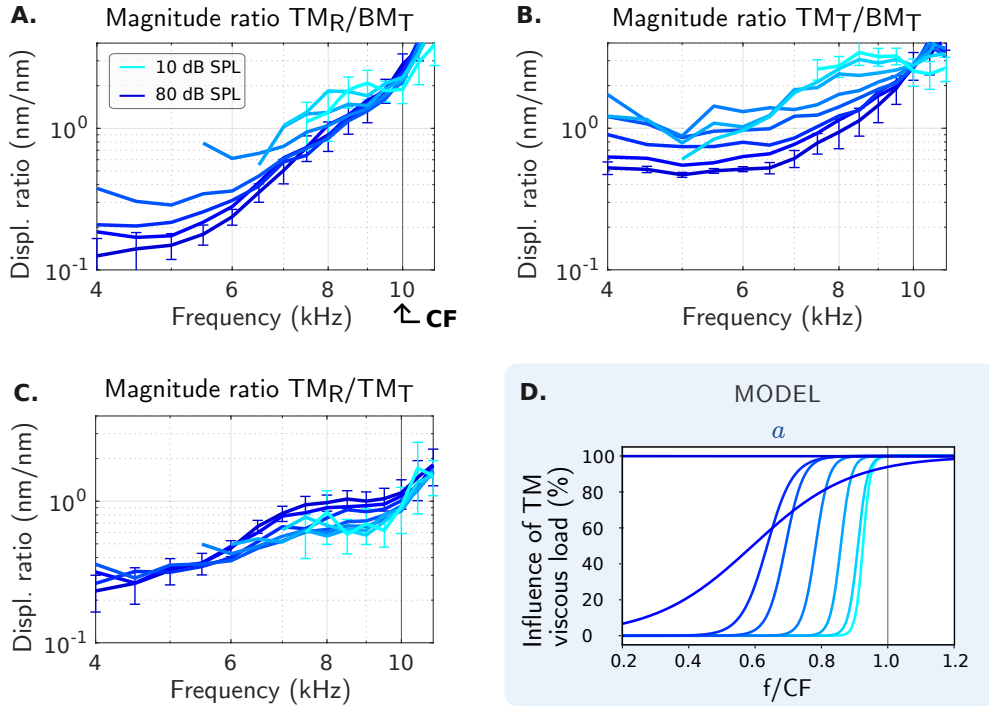


Figure 2: **A., B., C.:** OCT vibration data from Lee et al. [3]: displacement ratios in response to tones at one cochlear place ($CF = 10 \text{ kHz}$) averaged from $n=6$ CBA/CaJ mice. Ratios for both radial (subscript R) and transverse (subscript T) motions in 10-dB steps are presented. Standard errors (error bars) are shown for the lowest and highest sound levels. **D.** In the numerical simulations, a represents the influence of the TM viscous load on the BM admittance, which we set to vary with frequency and sound level (light to dark blue: 10 to 80 dB SPL). At a given sound level, $a(f/CF)$ is a sigmoid loosely fitting the radial-over-transverse displacement ‘boost’ in panel A (see subsection on deformation modes for further explanations).

transverse deformation. The corresponding pressure field is approximated by:

$$p_2(r, z) \propto (z_0 - z) \exp(-k'_r r), \quad (5)$$

with zero second derivative along the transverse direction. The incompressibility (Eq. 3) is expressed this time by $k'_r = k$.

OCT data of TM motion *in vivo* is scarce due to the low reflectivity of the TM. However, Lee et al. [3] provided data of TM motion in the mouse that could be consistent with the existence of two deformation modes in the short-wave region (reproduced in Fig. 2). The primary observation is that TM radial displacement, relative to BM transverse displacement, is enhanced at low sound levels in specific frequency regions (Fig. 2A). Our analysis suggests that TM radial motion is proportional to the radial derivative of the pressure field, equal to $-k_r p$ (for Eq. 4) or $-k'_r p$ (for Eq. 5) depending on the mode of motion. In the active mode, k'_r is equal to the wavelength k , which is higher than k_r in the passive mode by a factor $\sqrt{2}$,

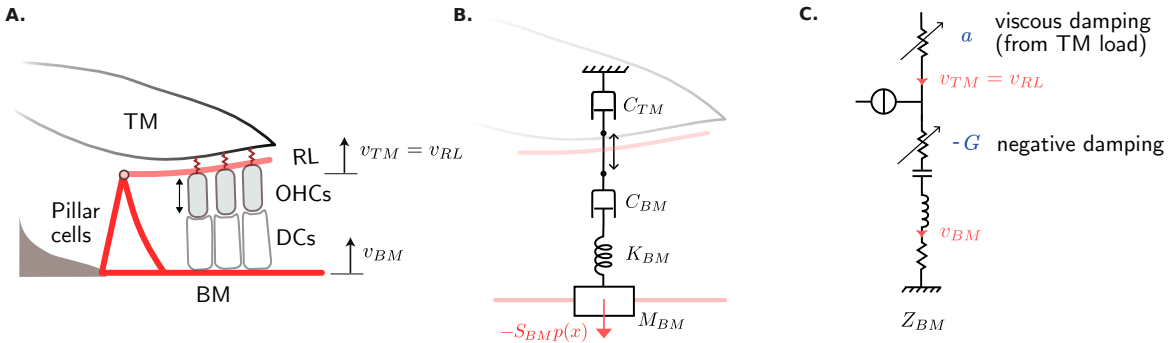


Figure 3: Several diagrams showing the simplification steps leading to the modeling of the BM impedance with lumped elements. **A.** Two degrees-of-freedom (DoF) view of cochlear micromechanics reducing the system to two transverse velocities (v_{BM} and v_{TM}). Red part=the stiff ‘frame’. DC=Deiter cell. **B.** Lumped-element mechanical model. The TM impedance is limited to a damper. The mass of the system is reduced to M_{BM} . **C.** Electrical circuit analogy. In addition to the RLC elements corresponding to a passive harmonic oscillator, the impedance includes a variable negative resistance, a velocity generator (simulating the vibration ‘hotspot’ [4] of the OHC region), and a variable resistor modeling viscous damping from the TM load. The parameters a and G (not homogeneous to mechanical resistance) in blue set the state of the BM impedance, transitioning from passive to active states. In the numerical simulations, a follows the sigmoid functions plotted in Fig. 2D, while G is linearly varied between two extremum values.

or +3 dB. This enhancement is a consequence of the near-incompressibility of the TM, and can be interpreted as a conversion of deformation in both directions into radial deformation alone when transverse deformations are suppressed by the active process. In this view, radial deformations (proportional to k^2) are doubled in magnitude from the passive to active state, but radial motion (either defined by velocity or displacement) is proportional to k , which explains why the enhancement factor is only $\sqrt{2}$. Assuming that the ratio of local pressure to BM velocity remains the same, irrespective of the sound level, this would agree with the observed enhancement of radial TM motion over transverse BM motion at low sound levels, in the frequency region where amplification is thought to occur (light vs dark blue plots in Fig. 2A).

A secondary, more speculative observation concerns the ratio of radial to transverse displacement in the TM. At high sound levels, in the frequency region below CF (7 kHz to 10 kHz), the two motion components are equal in magnitude (Fig. 2C, data averaged over several mice). This is consistent with the characterization of the passive mode of motion (Eq. 4), which predicts similar amplitude for the radial and transverse components. In the active mode, however, the radial and transverse velocities become uncoupled: deriving Eq. 5, we find that their ratio is $k'_r(z_0 - z)$, which depends on a free parameter z_0 . This implies that the individual velocity components could be influenced by different factors. The radial deformations in our analysis are connected to the existence of a compression wave in the TM (assumption underlying Eq. 3), while transverse motion in the active state would be more tightly connected to the transverse motion ‘hotspot’ [4] observed in the OHC region at low sound levels. This could explain why

transverse TM displacement is significantly larger than radial TM displacement in the 7 to 10 kHz region at low sound levels (light blue plots in Fig. 2C).

Based on the above interpretation of the OCT data, we can evaluate at which sound levels and in which frequency regions the active process is thought to be effective in suppressing TM deformations. To do so, we introduce a variable a , ranging from 0 to 1, quantifying the impact of the active process on the viscous load. $a = 1$ corresponds to the passive mode, where transverse viscous damping remains fully intact, while $a = 0$ represents the most active state, where TM transverse deformations and the related viscous damping are entirely suppressed. Intermediate values represent linear combinations of both modes. At a given sound level, we set a as a sigmoid function of f/CF , where CF is the best frequency of the BM response at hearing threshold at one given cochlear location. Fig. 2D displays the functions $a(f/CF)$ corresponding to the sound levels from the Lee et al. dataset, using the same color code. The sigmoid parameters were adjusted based on our interpretation of the displacement ratio enhancements shown in Fig. 2A. The rest of the paragraph describes the steps of the fitting process. First, the values in Fig. 2A were divided by the values corresponding to the highest sound level. If we denote the displacement ratio TM_R/BM_T by R , curves for R/R_{passive} were then obtained. Next, the values below 1 or above $\sqrt{2}$ were trimmed to have only values in the range $[1, \sqrt{2}]$. Each curve was then fitted by a function $func(f/CF) = \sqrt{2} + (1 - \sqrt{2}) \frac{1}{1 + \exp[-P1 \cdot (f/CF - P2)]}$ with $P1$ and $P2$ determined using a least-squares method. After fitting, a was defined as the logistic function appearing in $func$.

2.3. Mechanical model and BM admittance

In the rest of the Methods section, we describe how we simulated traveling waves using a mathematical approximation while accounting for the proposed mechanism. The key steps are outlined as follows:

1. Based on the analysis developed in the previous subsections, we derive an expression for the viscous force generated at the TM surface.
2. We incorporate this viscous force into an equivalent BM admittance formula, motivated by simple mechanical arguments.
3. We integrate the BM admittance into a transmission-line model and simulate traveling waves in response to tones using the WKB approximation.

In this subsection we derive a formula for the BM admittance in both passive and active scenarios (steps 1 and 2).

We start by considering a simplified model of cochlear micromechanics with two degrees of freedom (DoF), corresponding to Fig. 3A. One DoF is the transverse velocity v_{BM} and the second is the transverse velocity of the reticular lamina v_{RL} . The latter is assumed to be identical to v_{TM} , consistent with the motion between the TM and RL being essentially radial [13]. In the absence of TM viscous load, we still assume the presence of a classical anti-damping term, represented by a negative resistance in the BM impedance (Fig. 3C). We do not specify the mechanism leading to negative damping, as our focus is on the hypothetical



‘second’ mechanism controlling TM transverse damping. BM damping in the absence of TM viscous load is denoted by Γ , and can be expressed as the sum of a passive and active term, as in Sisto et al. (2021): $\Gamma = \Gamma_p + \Gamma_a$ with $\Gamma_p = \omega_{BM}$ and $\Gamma_a = -G\omega_{BM}$. The variable G represents the strength of negative damping achieved by the active process.

To incorporate the viscous forces acting on the TM in the BM admittance, we make the strong assumption that these forces do not exert work on the RL in the reference frame of the BM. This assumption is valid if OHC electromotility compensates for all the viscous load from the TM, so that the quantity $v_{RL} - v_{BM}$ remains of constant amplitude irrespective of the amount of viscous damping. Conceptually, this translates into modeling the action of OHCs as a ‘velocity generator’ (Fig. 3B), akin to a current generator in an electrical analogy (Fig. 3C). The consequence of this assumption for the 2 DoF model is that the viscous forces acting on the TM are entirely transferred to the BM mass moving with velocity v_{BM} . Our model does not make other assumptions on the mechanical coupling between the RL and BM. The route of transmission could involve the RL and the pillar cells, or the OHCs and the DCs — or both [13] — but it is not specified. We take this simplification one step further by considering that v_{TM}/v_{BM} remains constant across stimulus frequency, effectively reducing the model to 1 DoF. We consider, however, that the ratio v_{TM}/v_{BM} depends on the intensity of the stimulation (see next subsection).

To evaluate the viscous force F_V acting on the TM in the passive case, we use the analysis of deformation modes that was presented in the previous subsection. By letting v_{TM} be the transverse velocity of the lower part of the TM, the exponential profile of the pressure field over the transverse direction (Eq. 4) gives $\frac{\partial u_z}{\partial z} = -k_z v_{TM}$ on the lower surface of the TM. On the upper surface, Eq. 4 yields: $\frac{\partial u_z}{\partial z} = -k_z e^{-k_z H_{TM}} v_{TM}$, where H_{TM} is the height of the TM. Considering the simplified rectangular geometry described earlier and assuming once more that the viscous stress is divergence-free within the TM bulk, we derive the viscous force as

$$F_V = -2 \mu_{TM} S_{TM} (1 - e^{-k_z H_{TM}}) k_z v_{TM}. \quad (6)$$

F_V is the viscous force acting on the TM in the passive deformation mode. To include the other modes, F_V is multiplied by a , the variable introduced in the previous subsection. When a is decreased from 1 to 0, the system goes from the fully active to passive mode of deformations in the TM. In the simplified description of mechanics introduced above, the viscous force acting on the TM is transferred to the BM with the same magnitude. The new viscous term is included in a mass-spring-damper model which relates BM velocity to local forces:

$$S_{BM} \sigma_{BM} (-\omega^2 + j\omega\Gamma + \omega_{BM}^2) \frac{v_{BM}}{j\omega} = -p_d(z=0) S_{BM} + a F_V, \quad (7)$$

where σ_{BM} is the BM surface density. The modified BM admittance is therefore:

$$Y_{BM} = -\frac{j\omega}{\sigma_{BM} \tilde{\Delta}} \text{ with } \tilde{\Delta} = -\omega^2 + j\omega \left[\Gamma + 2a \frac{\mu_{TM}}{\sigma_{BM}} (1 - e^{-k_z H_{TM}}) k_z \frac{S_{TM}}{S_{BM}} \frac{v_{TM}}{v_{BM}} \right] + \omega_{BM}^2, \quad (8)$$



where it can be noted that the admittance depends on the wavelength (with $k_z = k/\sqrt{2}$). The admittance can be modified by tuning G , a , or both: G is a scalar variable controlling the classical damping term (with $\Gamma = (1 - G)\omega_{BM}$), and a is a function of frequency that sets the strength of the non-standard damping term from the TM viscous load.

2.4. Numerical simulations

The framework for simulating v_{BM} responses is a transmission-line model, where the fluid impedance and the BM admittance serve as series and shunt elements, respectively [27]. The model includes 2-D effects through the integration of pressure focusing [19] and cochlear guide tapering. The corresponding equations are reviewed below.

Defining $p_d = p(z) - p(-z)$ as the pressure difference between the scalae above the BM and the scala tympani, $\bar{p}_d = 1/H \int_0^H p_d dz$ as the averaged differential pressure and $U = \int_0^H u_x dz$ as the volume velocity in the upper scalae, the equations on averaged pressure and volume velocity are [28]:

$$H \frac{\partial \bar{p}_d}{\partial x} = -(Z_f H) U \quad (9)$$

$$\frac{\partial U}{\partial x} = v_{BM} = Y_{BM} p_d(z = 0^+) = \alpha Y_{BM} \bar{p}_d, \quad (10)$$

where H is the (semi-)height of the cochlea and $Z_f = \frac{2j\omega\rho}{H}$. Note that in the first equation, $Z_f H$ is independent of H . The second equation includes the factor $\alpha = p_d(z = 0^+)/\bar{p}_d$, which accounts for the focusing of the pressure around the BM in the short-wave region [19]. The following formula can be derived for α considering a local solution to Laplace's equation [28, 19]:

$$\alpha = \frac{kH}{\tanh kH}. \quad (11)$$

Combining Eq. 9 and Eq. 10, a variant of Webster's horn equation is obtained [29]:

$$\frac{1}{H} \frac{\partial}{\partial x} \left(H \frac{\partial \bar{p}_d}{\partial x} \right) = -Z_f Y_{BM} \alpha \bar{p}_d = -k^2 \bar{p}_d. \quad (12)$$

A WKB approximation of the forward-pressure wave, solution of the equation above, is [29]:

$$\bar{p}_d(x) = \bar{P}_0 \sqrt{\frac{H_0}{H}} \sqrt{\frac{k_0}{k}} \exp \left(-j \int_0^x k(x') dx' \right), \quad (13)$$

which can be evaluated by dividing the cochlear partition into $N_{sections}$ and considering the cumulative sum of $k(x')$ instead of the integral. The BM velocity can be derived from \bar{p}_d using the relation $v_{BM} = Y_{BM} \alpha \bar{p}_d$.



To apply Eq. 13 to our model, the wavenumber k must be determined. From the wave equation (Eq. 12), we have $k^2 = Z_f Y_{BM} \alpha$. Substituting the BM admittance with Eq. 8, we get the dispersion relation:

$$k^2 = \frac{2\alpha\omega^2\rho}{\sigma_{BM}H\left(\omega_{BM}^2 - \omega^2 + j\omega\left[\Gamma + 2a\frac{\mu_{TM}}{\sigma_{BM}}(1 - e^{-k_z H_{TM}})k_z\frac{S_{TM}v_{TM}}{S_{BM}v_{BM}}\right]\right)}. \quad (14)$$

To obtain a numerical value, we used the recursive procedure described in Sisto et al. [19], empirically converging for the range of values of interest for the simulation of the traveling wave. The procedure was initialized with the value obtained for $a = 0$ and $\alpha = 1$ (non-recursive formula). We then recursively updated k by taking the square root of the right-hand side in Eq. 14. This operation was repeated 30 times.

Table 1 lists the model parameters for simulating the forward-pressure wave. When it was possible, the parameters were set to reflect the anatomy of the mouse cochlea. This includes the place-frequency mapping defined by a Greenwood function [30]. In the version presented in this paper, the height of the cochlear ducts and the BM surface density are made place-dependent with $H \leftarrow \frac{\omega_{BM}}{\omega_0}H_0$, and $\sigma_{BM} \leftarrow \frac{\omega_0}{\omega_{BM}}\sigma_0$. This choice corresponds to a tapered guide [29] with a property of scaling symmetry on Z_f and $Z_{BM} = Y_{BM}^{-1}$, i.e., both impedances can be expressed in terms of the variable $s = j\omega/\omega_{BM}$ [27]. Note that this does not imply that the full model is scaling symmetric. In particular, the wavenumber k cannot be expressed with s alone, since it also depends on α scaling with ω_{BM} : the pressure focusing factor is stronger at the cochlear base than at the apex [29].

A point that needs to be noted is that $\omega_{BM}/(2\pi)$, the local resonance frequency determined by mass and stiffness, is not the same as CF, the best frequency at hearing thresholds. This difference arises because the traveling wave is dissipated before it reaches its characteristic place due to the high viscosity encountered in the short-wave region [19, 31]. The ratio $2\pi \cdot CF/\omega_{BM}$ was found to be approximately 0.56 based on simulations in which this parameter was iteratively adjusted. This correction factor influenced the model in two ways: it was used to scale the Greenwood function expressed in terms of ω_{BM} instead of CF , and it allowed a to be expressed as a function of ω/ω_{BM} instead of f/CF .

To reproduce the compressive behavior of the traveling wave with increasing levels of stimulation, we varied the parameters G , a , and v_{TM}/v_{BM} across simulations. The parameter choices were informed by OCT data in the mouse ($CF = 10$ kHz) for sound levels ranging from 10 dB to 80 dB [3]. We previously explained why and how a was fitted to the data on radial TM motion (see Fig. 2D and subsection on deformation modes). Similarly, v_{TM}/v_{BM} was linearly decreased from 3 to 1.7 based on the transverse motion data (Fig. 2B). The negative damping factor G was simultaneously decreased from 1.3 to 0.5 to match the dynamic range of the BM response. Note that we did not take into account any phase difference between v_{TM} and v_{BM} in the version presented in this paper.



Parameter	Value
cochlear height H	$170 \times 10^{-6} \text{ m}$ [32]
TM height H_{TM}	$25 \times 10^{-6} \text{ m}$
cochlear length L	$6 \times 10^{-3} \text{ m}$ [32]
surface ratio S_{TM}/S_{BM}	0.25
BM surface density σ_{BM}	$6 \times 10^{-2} \text{ kg m}^{-2}$
Fluid density ρ	$1 \times 10^3 \text{ kg m}^{-3}$
Dynamic viscosity μ_{TM}	$150 \times 10^{-3} \text{ Pa s}$ [21]
Characteristic pulsation ω_{BM}	$1.356 \times 10^6 e^{-826.56x} \text{ rad s}^{-1}$ [30, 32]
$2\pi \cdot \text{CF}/\omega_{BM}$	0.56
$N_{sections}$	1,000
G (negative damping)	1.3 to 0.5 (linearly decreased)
a (strength of non-standard viscous damping)	See Fig. 2D
v_{TM}/v_{BM}	3 to 1.7 (linearly decreased)

Table 1: Simulation parameters. For the parameters that depend on the cochlear location (height and BM surface density), the values corresponding to the place with $\omega_{BM} = 2\pi \cdot 10 \text{ kHz}$ are shown.

3. Results

We simulated the traveling wave in response to a 10-kHz probe tone with different strengths of the active process, roughly representing responses to sound levels from 10 to 80 dB SPL in mice. The spatial magnitude responses are shown in the upper panel of Fig. 4. The curves are normalized to the response magnitude at the cochlear base to show the compression of the peak response with increasing stimulation levels.

The left panel (Fig. 4A) shows the simulated traveling waves when the model does not include the control mechanism of the TM viscous load. In this figure, only the negative damping factor G is varied. The colored lines correspond to the responses with the admittance including the TM viscous load from the passive mode ($a = 1$). For comparison, the paler lines show the responses without the TM viscous load ($a = 0$), but including the viscous fluid stress acting on the BM [20] (with $\mu_w = 1 \text{ mPa s}$) to ensure that the model is stable. Comparing the two set of responses demonstrate the stronger effect of the TM viscous load compared to cortilymph viscosity acting at the BM interface. To achieve a comparable effect, one would need to increase the fluid viscosity to approximately $12 \mu_w$ (not shown). Viscous damping due to the presence of transverse velocity gradients is formally different from constant ratio damping because the associated viscous forces, relative to the BM velocity, depend on position and frequency. In box models, the pressure field follows a transverse exponential decay with a characteristic height of $1/k_z$, so that the transverse velocity gradients scale with the wavenumber sharply increasing



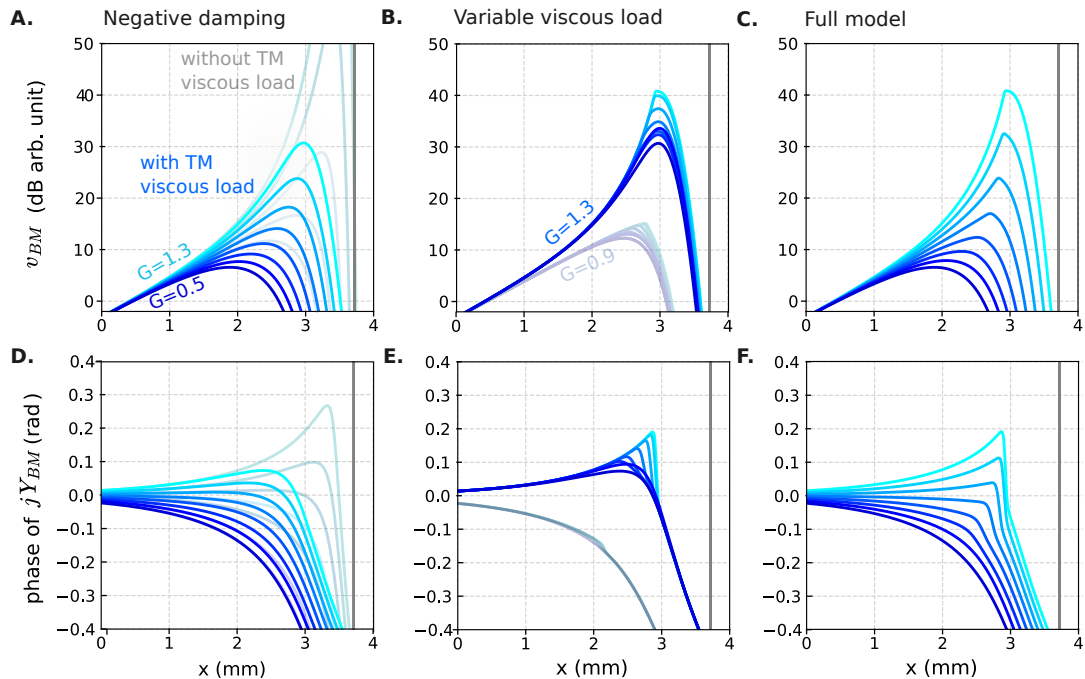


Figure 4: Simulation of BM velocity with the WKB method: responses to a tone ($f_p = 10$ kHz) with various strengths of the active process. x refers to the place on the cochlear partition from base to apex. **Top:** Magnitude of BM velocity normalized to BM velocity at the base of the cochlea. **Bottom:** Phase of jY_{BM} for the same responses. Left panel (A., D.): Only the negative damping term was linearly decreased, from $G = 1.5$ to $G = 0.5$. Responses in blue were obtained by including the TM viscous load in the model, without any reduction from OHC activity. Responses without the TM viscous load but with inclusion of fluid viscosity are shown with the paler lines (note: the curves for the three lowest G values overlap with the full-color ones). Center panel (B., E.): The negative damping factor (G) was fixed but the TM viscous load was varied as a function of frequency and level as indicated in Fig. 2D. The responses are shown for $G = 1.3$ (maximum value) and for a lower value (paler lines, $G = 0.9$). Right panel (C., F.): Simulations with the full model (negative damping + varying viscous load). G and the viscous load were varied in the same way as in the left and center panels (resp.). In all panels: the vertical gray line corresponds to the cochlear place where $\omega_{BM} = 2\pi f_p$.

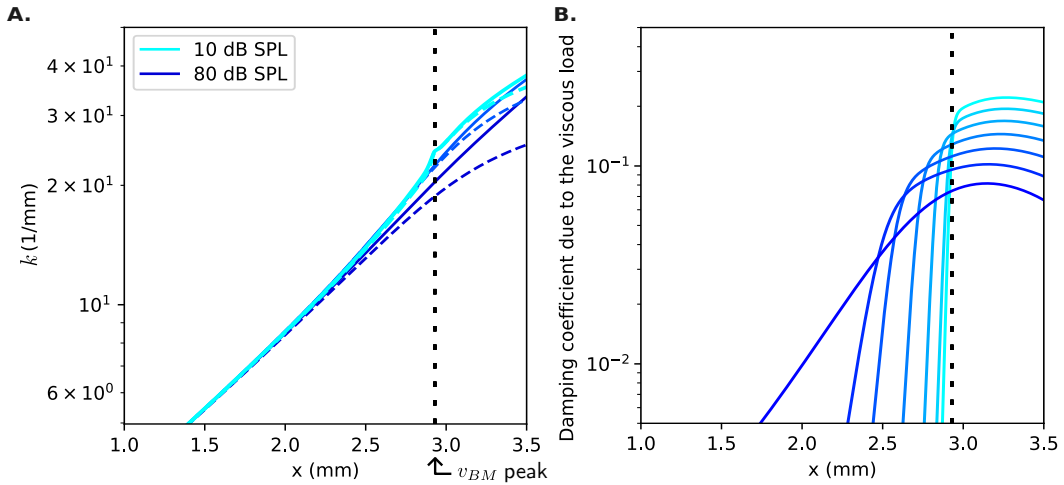


Figure 5: Wavenumber k and damping coefficient ζ corresponding to the traveling waves in Fig. 4C. ζ only reflects the damping contribution from the TM viscous load. It is a dimensionless factor analogous to a damping ratio, calculated as the real part of $aF_v/(Cv_{BM})$, where $C = 4\pi\sigma_{BM}S_{BM}f_p$. The plots for k are displayed for three levels: the minimum intensity (corresponding to $G = 1.3$), an intermediary level (50 dB, $G = 1$), and the maximum intensity ($G = 0.5$). The magnitude of k is shown as a solid line; the real part is shown as a dashed curve. Note that the y-scale for ζ changes by two orders of magnitude when it changes by one for k , making it possible to compare the trends for ζ and k^2 .

in the peak region [20]. Fluid viscosity results in a viscous stress on the BM proportional to k . The force due to TM viscoelasticity even scales with k^2 under the approximation $k_z H_{TM} \ll 1$, because of the difference $1 - e^{-k_z H}$ appearing in Eq. 6. Fig. 5 displays the damping coefficient, proportional to F_v/v_{BM} , alongside k^2 , making it possible to compare their trends. Viscosity has a stabilizing role by counteracting the build-up of pressure and BM velocity along the traveling wave. This effect is illustrated by Fig. 4A: without the TM viscous load, the BM velocity exhibits a steep and poorly controlled growth as the wave approaches its nominal characteristic place (marked as a vertical line). For the same variations in the G factor, the responses including the TM viscous load show smaller variations in the peak magnitude. Additionally, the wave peak is found basal to the nominal characteristic place, and the basal shift of the peak response between the most active and passive states is reduced. These observations align with the remarks on the role of fluid viscosity in Sisto et al. [19, 31].

The center panel (Fig. 4B) corresponds to the reciprocal simulation settings, where the negative damping factor G is kept constant, but the TM viscous load is modulated according to the curves in Fig. 2D. In these simulations, v_{TM}/v_{BM} was fixed at its maximum value of 3 and G at its maximum value of 1.3 to show the maximal effect of varying the viscous load. This effect is characterized by a modulation of the peak response up to 10 dB. Outside the peak region, the modulation of the viscous load has no visible impact. The localized nature of the effect is explained by two factors: viscous damping is significantly enhanced in the short-wave

region; and modulation of the viscous load predominantly occurs in the region slightly basal to the peak (Fig. 2D). Fig. 4B also displays the responses with a lower value of G ($G = 0.9$; paler lines), corresponding to a slightly damped system. Under these conditions, the effect of the variable viscous load is reduced to 30% to 50% of the maximum effect. If G is fixed to its minimum value ($G = 0.5$), the effect on the response becomes even indiscernible (differences in peak magnitude less than 1 dB; not shown). This demonstrates that negative damping ($G > 1$) is necessary for the control of the viscous load to have a substantial effect. If the wave is sufficiently undamped, a large part of the wave energy reaches the short-wave region, where variations in viscosity can strongly affect the peak. Otherwise, the peak region is shifted basally in a region where viscous damping is too low to have an impact on the response.

In the simulations with the full model, shown in the right panel (Fig. 4C), negative damping and modulation of the viscous load combine to generate a tall peak in response to a low-intensity sound. This is achieved while maintaining a limited spatial shift of the peak when the sound level is increased, corresponding to a half-octave (Fig. 7). Figures 5 and 6 display complementary information to v_{BM} for the WKB simulations carried out with the full model. Figure 6 highlights the contributions of the different factors to the computation of v_{BM} . It demonstrates that the predominant factor to the shape and compression of the wave is the exponential factor appearing in the computation of \bar{p}_d (Eq. 13). The magnitude of the BM admittance at the peak of the wave is reduced by only 1.6 dB when transitioning from the most active to most passive state (20 % change). A comparable relative change is observed for the magnitude of the wavenumber (Fig. 5). The real part of the wavenumber, ranging from 24 to 19 per mm at the peak, determines the wavelength, which varies between 0.26 mm to 0.33 mm at the peak. Although the variations in the modulus are small, the phase of Y_{BM} has a big impact on the magnitude of $e^{-j \int k(x')dx'}$. In the lower panel of Fig. 4, we presented the phase of jY_{BM} , equal to the phase of k in the short-wave region (or k^2 in the long-wave region) [19]. The overall trend shows that it becomes increasingly negative with higher sound levels or approaching the characteristic place, reflecting in both cases a shift toward more dissipative states. When the system is subject to negative damping (reflected as a positive phase in jY_{BM}), the control of the viscous load limits or unleashes its effect in a small region basal to the peak (Fig 4E). This can lead to an abrupt transition of the phase in the peak region, also visible for the simulations with the full model (Fig 4F).

The results described so far involved one probe tone and a continuum of cochlear locations. We can also simulate responses to multiple tones at a specific cochlear location, which more closely matches experimental data. Figure 7 shows the results of such simulations at the cochlear place with CF = 10 kHz, overlaid on OCT vibration data in mice. The experimental data are from the Lee et al. dataset, which was independently used in the Methods section to calibrate key model parameters, including the spatial modulation of the viscous load (parameter a , Fig. 2). The values for the negative damping factor G represent the same range as in the previous simulations, but were fine-tuned to provide the best fit to the experimental curves. An excellent match is observed between the simulated and actual data for frequencies below CF. For frequencies above CF, the actual data exhibit a steeper roll-off at low and medium



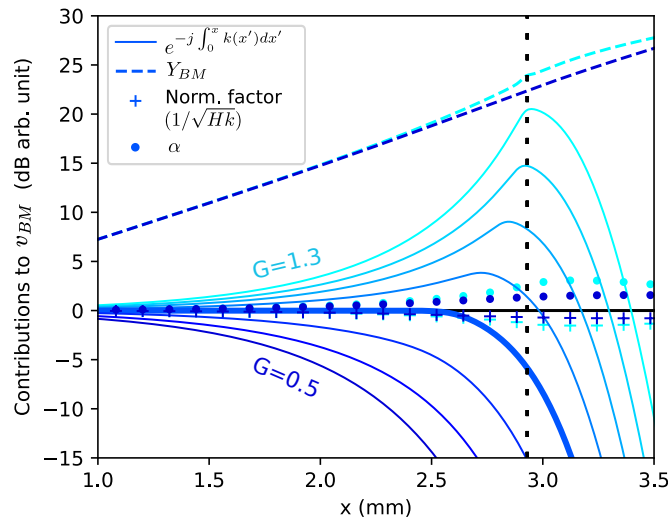


Figure 6: Contributions to the spatial profile of v_{BM} (WKB simulations with the full model corresponding to Fig. 4C). The term $e^{-j \int k}$ and the normalization factor appear in the WKB approximation of \bar{p}_d (Eq. 13). v_{BM} is obtained by multiplying \bar{p}_d by α and Y_{BM} . The thick line for $e^{-j \int k}$ corresponds to $G = 1$ (no gain or loss of power in the absence of viscous loss). Each curve is normalized to its value at the base of the cochlea ($x = 0$). All stimulation levels are shown for $e^{-j \int k}$, while the other curves are displayed only for the minimum and maximum intensities.

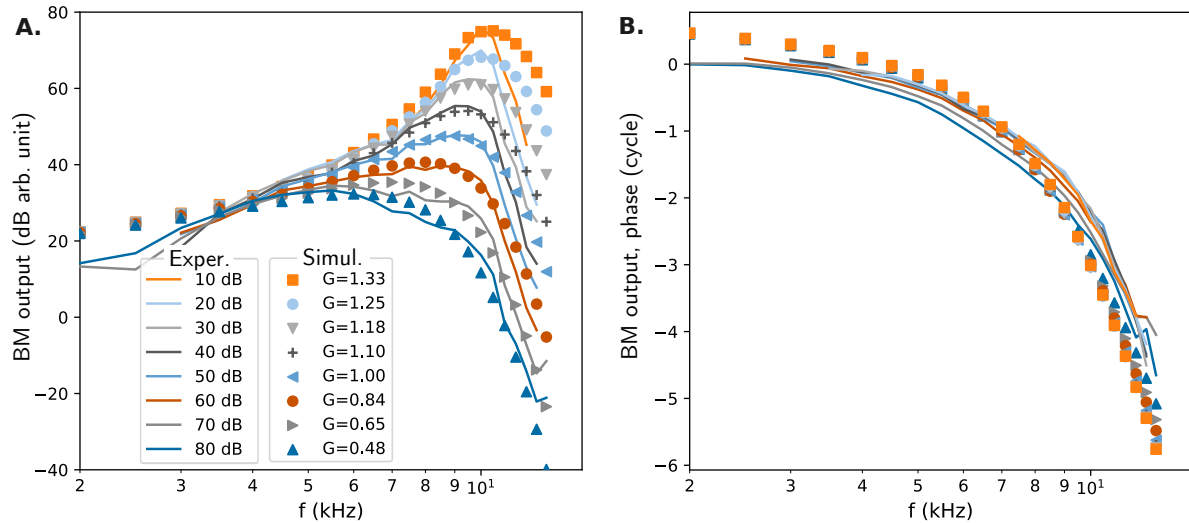


Figure 7: **A.** Simulation of BM velocity (symbols) in response to tones at a specific cochlear location (CF = 10 kHz). The response magnitude is compared with experimental data, in solid lines (BM displacement gain re:middle ear averaged over 6 mice, from Lee et al. 2016). The values for G , which sets the negative damping in the simulations, were adjusted to provide the best fit at each sound level. The viscous load was varied as in Fig. 2D and Fig. 4C. Sound levels for the experimental data are in dB SPL. The y-axis values for the Lee et al. data are the same as originally reported, while the simulation results were vertically shifted to compare the two data sets. **B.** Corresponding phase responses.

sound levels. In supplementary materials, we provide a figure showing the comparison with the Lee et al. data using other model versions (Fig. S1). The response below CF is not captured by a model including only the effect of fluid viscosity, even if the viscosity is increased to $5\mu_w$, though it achieves the correct roll-off for frequencies above CF. However, an equally good fit for frequencies below CF can be obtained by including the TM passive load, with no mechanism for varying the TM load, but with higher G values.

4. Discussion

This paper introduced the hypothesis that the cochlear active process could modulate traveling-wave viscous losses via the cancellation of TM transverse deformations. Several arguments of different nature were provided in support of this hypothesis. The central arguments were: in the passive state, a transverse velocity gradient in the TM is expected due to the exponential decay of the fluid pressure above the BM; in the active state, this gradient may be compensated by a velocity gradient observed experimentally in the region of OHCs. Secondary arguments included structural or mechanical properties such as the orientation of collagen fibers in the TM, as well as vibration data potentially corresponding to two deformation modes in the TM in the region basal to the peak (Fig. 2). A simplified mechanical model of the organ of Corti was used to derive a BM equivalent admittance which included a viscous damping

term originating from the TM load. This allowed us to compute WKB approximations of the traveling wave with different strengths of the active process. With realistic parameter values (TM dynamic viscosity, TM height, etc.), the simulations showed that the proposed mechanism could have a significant effect on BM velocity in the peak region (Fig. 4C). The model provided an excellent match with experimental data on BM velocity, but only for frequencies below CF (Fig. 7A). A more realistic supra-CF roll-off might be obtained by taking into account the phase shift of the RL over the BM in the CF region (not integrated in the current model), but this point is still under investigation.

We saw that to obtain these results, a varying term representing negative damping was still required in the model admittance. As the negative damping term is increased (through the factor G), the peak response spans a large dynamic range, but also the effect of undamping from the TM varying load is stronger (Fig. 4B). These observations led us to hypothesize the coexistence of two mechanisms contributing to traveling-wave amplification: a first mechanism of negative damping and a second mechanism of viscous undamping. The origin of the ‘first’ mechanism is not addressed in this paper but it could correspond to proposals developed elsewhere [14, 15, 33, 34].

What could be the possible advantages of this second mechanism? First, it could limit the extent of negative damping required to achieve a large dynamic range of responses, thereby limiting potential instability issues. Second, although the maximum modulation of BM velocity observed in our simulation appears quite modest (around 10 dB), it is already sufficient to modify the morphology of the peak (compare Fig. 4A and Fig. 4C), providing additional control over the response in the short-wave region. Remarkably, the modulation of the viscous load alone affects the BM velocity magnitude but is not associated with a basal or apical shift of the wave peak (Fig. 4B). This behavior is reminiscent of the reduction in response gain induced by the medial olivocochlear reflex: when the olivocochlear efferents are activated, the thresholds of auditory nerve tuning curves are raised, but the center frequencies stay virtually the same [35]. The proposed mechanism also offers a solution to the problem of ‘propagating’ versus ‘non-propagating’ amplification, which has recently received much attention [5, 7, 14, 36]. This question arises from the observation that while compressive nonlinearities in the OHC region exhibit broadband characteristics, traveling-wave amplification builds up only in a restricted region basal to the peak. This is commonly interpreted as the existence of a physical process that acts as a filter, allowing only a narrow frequency range of the power locally injected by the OHCs to effectively couple to the traveling wave. The proposed mechanism naturally reproduces this behavior: even if TM deformations are suppressed across all frequencies, the effect on the traveling wave is confined to the short-wave region, where viscous forces are most prominent (Fig. 4B).

The simulated spatial patterns of BM velocity have features in common with the WKB simulations in Sisto et al. [19, 20], which did not include TM viscoelasticity but did include fluid viscosity. In their simulations, the viscosity constant had to be set to 10 times the viscosity of water in order to obtain a significant effect of fluid viscosity on the traveling wave. Viscoelasticity within the organ of Corti was already suggested as a plausible argument for



the use of an increased viscosity constant. We obtain an effect of similar size, but it is not immediately evident from F_V (Eq. 6) why this is the case. Compared to the viscous force at the BM-fluid interface in Sisto et al., F_V includes a difference between the stress on the upper and lower surface of the TM, which accounts for a factor $1 - e^{-k_z H_{TM}} \approx 30\%$ at the wave peak (the spatial variation of this factor is shown in supplementary figure Fig. S2). Another factor that reduces the magnitude of the viscous force is the smaller effective TM surface area relative to the BM surface area (we chose $S_{TM}/S_{BM} = 0.25$). F_V also lacks a factor of 2 compared to the expression in Sisto et al., as the TM is only present on one side of the cochlear duct, unlike the fluid. These factors collectively reduce the magnitude of the viscous force by around 30. This is offset by two enhancing factors: the dynamic viscosity of the TM —two orders of magnitude higher than that of water — and the velocity ratio v_{TM}/v_{BM} equal to 3 at the lowest sound level. This last observation highlights how the large relative motion of the TM, as seen in experiments, could play an important role in amplifying the proposed mechanism's effect.

Another common feature with the simulations in Sisto et al. is that the wave peak in response to a tone is found basal to the nominal characteristic place. This occurs because the traveling wave is heavily damped by viscous losses before reaching the resonance region [31]. In our simulations, the best frequency (CF in text) was lower than the local characteristic frequency $\omega_{BM}/(2\pi)$ by a factor of 0.56. This behavior differs from many traveling-wave models (e.g., Shera and Zweig [37]), in which the best frequency at a cochlear location coincides with the local BM characteristic frequency determined by the stiffness-to-weight ratio of the cochlear partition. This latter choice initially seems more natural, because the traveling-wave peak shares several features with the transition seen at a resonance. Models incorporating fluid viscous damping generally produce spatial responses for v_{BM} that appear too ‘rounded’ to be realistic (as seen in Sisto et al., or with full-color lines in Fig. 4A), because the peak occurs in the stiffness-dominated region, away from the actual resonance. Here, however, the specific form of the admittance and the proposed mechanism preserved most of the expected features of the traveling wave (Fig. 4C), especially the ‘peakiness’ of BM velocity excitation patterns and the limited basal shift of the peak with increasing sound levels. However, we were not able to reproduce the steep roll-off of BM velocity for frequencies above CF (Fig. 7A). The simulated responses were marked by an abrupt transition in the phase of the admittance at the wave peak (Fig. 4F), but with smaller phase values compared to a true resonance. This feature is not undesirable: because the variation of the admittance phase remains limited, it has little influence on the v_{BM} phase response. Consequently, the v_{BM} phase response is primarily set by the pressure wave and decreases steadily with stimulus frequency (Fig. 7B). For models in which the wave peak and characteristic place coincide, the phase varies too rapidly in the peak region, or the BM admittance must be carefully controlled [27]. Calibrating these engineered-admittance models is particularly challenging [37], as it requires ensuring the model's stability, controlling the phase response, and adjusting the v_{BM} magnitude response — the latter depending on both changes in pressure-wave gain and changes in the admittance magnitude. In comparison, the behavior of the model presented here is quite simple, as variations in the response are



largely accounted for by the spatial integral of the complex wavenumber (Fig. 6). Because the peak occurs in the stiffness-dominated region (i.e., where the BM reactance is still large), a change in damping does not affect the magnitude of the BM admittance by a large amount (by a maximum of 20% in our simulations). A relatively small change in BM admittance appears consistent with experimental data as investigators reported similar variations in BM velocity and pressure across sound levels [38].

The model in this paper corresponds to an ‘overturned’ model of active cochlear mechanics [15], where the RL is in phase or leads the BM by a small phase difference, rather than exhibiting a quarter-cycle lag as predicted by the push-pull hypothesis. This configuration appears more in line with recent OCT data — although the relative phase of the RL, and its compatibility with traveling-wave models, remains a topic of discussion [34]. Mechanically, this implies the seemingly counterintuitive idea that OHCs contribute to damping BM motion rather than injecting power into the traveling wave. However, the critique that OHCs need a mechanical support to have an effective action on the BM, often directed at the push-pull hypothesis, is also valid for the ‘overtuned’ description of cochlear mechanics. In this paper, we assumed that the transverse viscous resistance of the TM could provide the mechanical support required for an effective damping force on the BM. The strength of this resistance would however depend on the state of the active process. Under this framework, the role of the OHCs would be twofold. First, they would modulate the TM transverse viscous load by interfering with the velocity gradient within the TM. Second, they would locally compensate for the viscous damping that affects their motion, ensuring that the damping force targets BM motion rather than merely the relative motion between the OHCs and the BM, which would be counterproductive. In other words, the OHCs could facilitate the transfer of the generated damping force to the BM, ensuring that the BM admittance and traveling-wave propagation are maximally affected by the proposed mechanism of undamping.

The question of the mechanical support required for an effective damping force can be taken a step further. We treated the viscous forces as local, and simply considered the differences of the forces acting on the upper and lower surface of the TM. However, if the TM/BM complex is considered as a whole, the viscous forces are internal forces, and the sum of internal forces must be equal to zero. Any force opposing BM motion must eventually find its origin in an external element. This raises the question: where would the damping force described in this paper ultimately come from? The analysis is complex because, in addition to the forces associated with the transverse velocity gradients, there are shearing forces associated with radial or longitudinal variations in the transverse velocity — which were assumed to cancel the sum of viscous forces in the bulk of the TM (resulting in a divergence-free stress field). A possible answer is that the external damping force could come from the TM limbal attachment in the form of a change in shear stress.

The mechanical model and the description of forces involved were highly simplified, relying on many assumptions to facilitate an analytical approach. One crucial assumption was that the transverse velocity in the TM exhibits an exponential-decay profile in the passive scenario, similar to the fluid flow above the BM in box models of the cochlea. This follows from the



Helmholtz-like equation (Eq. 3), derived in analogy to the Laplace's equation satisfied by the cochlear fluid. The underlying premise of this equation is that a wave propagates in the TM with longitudinal motion similar to that of the fluid pressure wave. Rather than being driven directly by the fluid, this wave could be driven by longitudinal oscillations in the organ of Corti. Recent studies have highlighted the importance of in-vivo longitudinal motion in the region of OHCs [4, 39], attached to the TM via the OHC hair bundles. However, to the authors' knowledge, no direct data confirms whether this longitudinal motion extends to the TM.

This work represents a first modeling approach that provides a useful framework for exploring the consequences of an undamping mechanism based on the viscoelasticity of the TM. Several improvements could refine the conclusions of this simplified approach, including more realistic representations of TM geometry and viscoelastic properties, non-ideal flow dynamics, integration of RL or TM motion phase relative to the BM, or a more accurate account of organ-of-Corti mechanics. The existence of the proposed mechanism could be further assessed by testing the model's predictions against a broader set of mechanical data, including measurements in mouse mutants with altered TM properties. Strong support for this hypothesis would eventually come from more direct experimental evidence, such as in vivo or ex vivo observations of TM deformation modes — although such experiments may be challenging due to the TM's low reflectivity and the small deformations involved.

Acknowledgements

This work was supported by the FWO grant “AudiMod” (G068621N). We thank the Oghalai lab for having publicly shared their dataset (<https://github.com/jso111/Lee2016>).

Author contributions

François Deloche: Conceptualization, Investigation, Methodology, Formal analysis, Software, Writing original draft. **Morgan Thienpont:** Software, Formal Analysis. **Renata Sisto, Arturo Moleti:** Supervision. **Sarah Verhulst:** Supervision, Project administration, Funding acquisition, Review and editing.

Code availability

The source code used to generate the results is available on the public repository [10.5281/zenodo.15380249](https://doi.org/10.5281/zenodo.15380249).

Declaration of AI-assisted technologies in the writing process

During the preparation of this work, FD used ChatGPT (OpenAI) and DeepL in order to improve the readability of the text. The corresponding changes were minor. After using these tools, the authors reviewed and edited the content as needed and take full responsibility for the content of the published article.



Declaration of interests

The authors declare no competing interests.

Supplementary material

Supplementary figures: *Fig S1.* Comparison of basilar membrane velocity (frequency responses of simulations and experimental data) using different models versions. *Fig S2.* Relative difference of stress (on lower/upper TM surface) as a function of cochlear place for a tone probe of 10 kHz.

References

- [1] M. A. Ruggero, N. C. Rich, A. Recio, S. S. Narayan, L. Robles, Basilar-membrane responses to tones at the base of the chinchilla cochlea, *The Journal of the Acoustical Society of America* 101 (4) (1997) 2151–2163. [arXiv:9566320](https://arxiv.org/abs/9566320), doi:[10.1121/1.418265](https://doi.org/10.1121/1.418265).
- [2] T. Ren, W. He, D. Kemp, Reticular lamina and basilar membrane vibrations in living mouse cochleae, *Proceedings of the National Academy of Sciences of the United States of America* 113 (35) (2016) 9910–9915. doi:[10.1073/pnas.1607428113](https://doi.org/10.1073/pnas.1607428113).
- [3] H. Y. Lee, P. D. Raphael, A. Xia, J. Kim, N. Grillet, B. E. Applegate, A. K. Ellerbee Bowden, J. S. Oghalai, Two-Dimensional Cochlear Micromechanics Measured In Vivo Demonstrate Radial Tuning within the Mouse Organ of Corti, *The Journal of Neuroscience* 36 (31) (2016) 8160–8173. doi:[10.1523/JNEUROSCI.1157-16.2016](https://doi.org/10.1523/JNEUROSCI.1157-16.2016).
- [4] N. P. Cooper, A. Vavakou, M. van der Heijden, Vibration hotspots reveal longitudinal funneling of sound-evoked motion in the mammalian cochlea, *Nature Communications* 9 (1) (2018) 3054. doi:[10.1038/s41467-018-05483-z](https://doi.org/10.1038/s41467-018-05483-z).
- [5] J. B. Dewey, B. E. Applegate, J. S. Oghalai, Amplification and Suppression of Traveling Waves along the Mouse Organ of Corti: Evidence for Spatial Variation in the Longitudinal Coupling of Outer Hair Cell-Generated Forces, *Journal of Neuroscience* 39 (10) (2019) 1805–1816. doi:[10.1523/JNEUROSCI.2608-18.2019](https://doi.org/10.1523/JNEUROSCI.2608-18.2019).
- [6] W. He, G. Burwood, E. V. Porsov, A. Fridberger, A. L. Nuttall, T. Ren, The reticular lamina and basilar membrane vibrations in the transverse direction in the basal turn of the living gerbil cochlea, *Scientific Reports* 12 (1) (2022) 19810. doi:[10.1038/s41598-022-24394-0](https://doi.org/10.1038/s41598-022-24394-0).
- [7] J. B. Dewey, A. Altoè, C. A. Shera, B. E. Applegate, J. S. Oghalai, Cochlear outer hair cell electromotility enhances organ of Corti motion on a cycle-by-cycle basis at high frequencies in vivo, *Proceedings of the National Academy of Sciences* 118 (43) (2021) e2025206118. doi:[10.1073/pnas.2025206118](https://doi.org/10.1073/pnas.2025206118).
- [8] M. van der Heijden, A. Vavakou, Rectifying and sluggish: Outer hair cells as regulators rather than amplifiers, *Hearing Research* 423 (2022) 108367. doi:[10.1016/j.heares.2021.108367](https://doi.org/10.1016/j.heares.2021.108367).
- [9] A. J. Hudspeth, Making an Effort to Listen: Mechanical Amplification in the Ear, *Neuron* 59 (4) (2008) 530–545. [arXiv:18760690](https://arxiv.org/abs/18760690), doi:[10.1016/j.neuron.2008.07.012](https://doi.org/10.1016/j.neuron.2008.07.012).
- [10] T. Reichenbach, A. J. Hudspeth, The physics of hearing: Fluid mechanics and the active process of the inner ear, *Reports on Progress in Physics* 77 (7) (2014) 076601. [arXiv:1408.2085](https://arxiv.org/abs/1408.2085), doi:[10.1088/0034-4885/77/7/076601](https://doi.org/10.1088/0034-4885/77/7/076601).
- [11] C. E. Stribu, Y. Wang, E. S. Olson, Manipulation of the Endocochlear Potential Reveals Two Distinct Types of Cochlear Nonlinearity, *Biophysical Journal* 119 (10) (2020) 2087–2101. doi:[10.1016/j.bpj.2020.10.005](https://doi.org/10.1016/j.bpj.2020.10.005).
- [12] J. J. Guinan, A. Salt, M. A. Cheatham, Progress in Cochlear Physiology after Békésy, *Hearing Research* 293 (1-2) (2012) 12–20. doi:[10.1016/j.heares.2012.05.005](https://doi.org/10.1016/j.heares.2012.05.005).



- [13] W. Zhou, T. Jabeen, S. Sabha, J. Becker, J.-H. Nam, Deiters Cells Act as Mechanical Equalizers for Outer Hair Cells, *Journal of Neuroscience* 42 (44) (2022) 8361–8372. [doi:10.1523/JNEUROSCI.2417-21.2022](https://doi.org/10.1523/JNEUROSCI.2417-21.2022).
- [14] J. J. Guinan, Cochlear amplification in the short-wave region by outer hair cells changing organ-of-Corti area to amplify the fluid traveling wave, *Hearing Research* 426 (2022) 108641. [doi:10.1016/j.heares.2022.108641](https://doi.org/10.1016/j.heares.2022.108641).
- [15] A. Altoè, J. B. Dewey, K. K. Charaziak, J. S. Oghalai, C. A. Shera, Overturning the mechanisms of cochlear amplification via area deformations of the organ of Corti, *The Journal of the Acoustical Society of America* 152 (4) (2022) 2227–2239. [doi:10.1121/10.0014794](https://doi.org/10.1121/10.0014794).
- [16] N. H. Cho, S. Puria, Cochlear motion across the reticular lamina implies that it is not a stiff plate, *Scientific Reports* 12 (1) (2022) 18715. [doi:10.1038/s41598-022-23525-x](https://doi.org/10.1038/s41598-022-23525-x).
- [17] C. E. Strimbu, L. A. Chiriboga, B. L. Frost, E. S. Olson, Regional differences in cochlear nonlinearity across the basal organ of Corti of gerbil: Regional differences in cochlear nonlinearity, *Hearing Research* 443 (2024) 108951. [doi:10.1016/j.heares.2024.108951](https://doi.org/10.1016/j.heares.2024.108951).
- [18] M. van der Heijden, C. P. C. Versteegh, Energy Flux in the Cochlea: Evidence Against Power Amplification of the Traveling Wave, *JARO: Journal of the Association for Research in Otolaryngology* 16 (5) (2015) 581–597. [doi:10.1007/s10162-015-0529-5](https://doi.org/10.1007/s10162-015-0529-5).
- [19] R. Sisto, D. Belardinelli, A. Moleti, Fluid focusing and viscosity allow high gain and stability of the cochlear response, *The Journal of the Acoustical Society of America* 150 (6) (2021) 4283–4296. [doi:10.1121/10.0008940](https://doi.org/10.1121/10.0008940).
- [20] R. Sisto, D. Belardinelli, A. Altoè, C. A. Shera, A. Moleti, Crucial 3-D viscous hydrodynamic contributions to the theoretical modeling of the cochlear response, *The Journal of the Acoustical Society of America* 153 (1) (2023) 77–86. [doi:10.1121/10.0016809](https://doi.org/10.1121/10.0016809).
- [21] R. Ghaffari, A. J. Aranyosi, D. M. Freeman, Longitudinally propagating traveling waves of the mammalian tectorial membrane, *Proceedings of the National Academy of Sciences* 104 (42) (2007) 16510–16515. [doi:10.1073/pnas.0703665104](https://doi.org/10.1073/pnas.0703665104).
- [22] L. R. Andrade, F. T. Salles, M. Grati, U. Manor, B. Kachar, Tectorins crosslink type II collagen fibrils and connect the tectorial membrane to the spiral limbus, *Journal of Structural Biology* 194 (2) (2016) 139–146. [doi:10.1016/j.jsb.2016.01.006](https://doi.org/10.1016/j.jsb.2016.01.006).
- [23] H. Hayashi, A. Schrott-Fischer, R. Glueckert, W. Liu, W. Salvenmoser, P. Santi, H. Rask-Andersen, Molecular organization and fine structure of the human tectorial membrane: Is it replenished?, *Cell and Tissue Research* 362 (3) (2015) 513–527. [doi:10.1007/s00441-015-2225-5](https://doi.org/10.1007/s00441-015-2225-5).
- [24] A. Niazi, J. A. Kim, D.-K. Kim, D. Lu, I. Sterin, J. Park, S. Park, Microvilli regulate the release modes of alpha-tectorin to organize the domain-specific matrix architecture of the tectorial membrane (Jan. 2024). [arXiv:10.1101/2024.01.04.574255](https://arxiv.org/abs/2401.04574), [doi:10.1101/2024.01.04.574255](https://doi.org/10.1101/2024.01.04.574255).
- [25] S. P. Weaver, L. Schweitzer, A radial gradient of fibril density in the gerbil tectorial membrane, *Hearing Research* 76 (1) (1994) 1–6. [doi:10.1016/0378-5955\(94\)90081-7](https://doi.org/10.1016/0378-5955(94)90081-7).
- [26] R. Gueta, D. Barlam, R. Z. Shneck, I. Rousso, Measurement of the mechanical properties of isolated tectorial membrane using atomic force microscopy, *Proceedings of the National Academy of Sciences* 103 (40) (2006) 14790–14795. [doi:10.1073/pnas.0603429103](https://doi.org/10.1073/pnas.0603429103).
- [27] G. Zweig, Finding the impedance of the organ of Corti, *The Journal of the Acoustical Society of America* 89 (3) (1991) 1229–1254. [doi:10.1121/1.400653](https://doi.org/10.1121/1.400653).
- [28] C. A. Shera, A. Tubis, C. L. Talmadge, Coherent reflection in a two-dimensional cochlea: Short-wave versus long-wave scattering in the generation of reflection-source otoacoustic emissions, *The Journal of the Acoustical Society of America* 118 (1) (2005) 287–313. [doi:10.1121/1.1895025](https://doi.org/10.1121/1.1895025).
- [29] A. Altoè, C. A. Shera, The cochlear ear horn: Geometric origin of tonotopic variations in auditory signal processing, *Scientific Reports* 10 (2020) 20528. [doi:10.1038/s41598-020-77042-w](https://doi.org/10.1038/s41598-020-77042-w).
- [30] D. D. Greenwood, A cochlear frequency-position function for several species-29 years later, *The Journal of the Acoustical Society of America* 87 (1990) 2592. [doi:10.1121/1.399052](https://doi.org/10.1121/1.399052).
- [31] R. Sisto, A. Moleti, The tonotopic cochlea puzzle: A resonant transmission line with a “non-resonant” response peak, *JASA Express Letters* 4 (7) (2024) 074401. [doi:10.1121/10.0028020](https://doi.org/10.1121/10.0028020).
- [32] M. Thienpont, F. Deloche, S. Keshishzadeh, D. Kiselev, J. Bourien, J.-L. Puel, B. Buran, N. Bramhall,



- S. Verhulst, Translating a Computational Model of the Human Auditory Periphery to Gerbil and Mouse for Comparative Auditory Research, in: Mechanics of Hearing Workshop 2024 (MoH 24), Zenodo, Ann Arbor, USA, 2024. [doi:10.5281/zenodo.13769392](https://doi.org/10.5281/zenodo.13769392).
- [33] Y.-J. Yoon, C. R. Steele, S. Puria, Feed-Forward and Feed-Backward Amplification Model from Cochlear Cytoarchitecture: An Interspecies Comparison, *Biophysical Journal* 100 (1) (2011) 1. [doi:10.1016/j.bpj.2010.11.039](https://doi.org/10.1016/j.bpj.2010.11.039).
- [34] R. Sisto, The experimental OHC elongation is not inconsistent with effective transfer of mechanical power to the BM, in: Mechanics of Hearing Workshop 2024 (MoH 24), Zenodo, 2024. [doi:10.5281/zenodo.13762200](https://doi.org/10.5281/zenodo.13762200).
- [35] J. J. Guinan, M. L. Gifford, Effects of electrical stimulation of efferent olivocochlear neurons on cat auditory-nerve fibers. III. Tuning curves and thresholds at CF, *Hearing Research* 37 (1) (1988) 29–45. [doi:10.1016/0378-5955\(88\)90075-5](https://doi.org/10.1016/0378-5955(88)90075-5).
- [36] E. Fallah, C. E. Strimbu, E. S. Olson, Nonlinearity and Amplification in Cochlear Responses to Single and Multi-Tone Stimuli, *Hearing Research* 377 (2019) 271–281. [doi:10.1016/j.heares.2019.04.001](https://doi.org/10.1016/j.heares.2019.04.001).
- [37] C. A. Shera, Intensity-invariance of fine time structure in basilar-membrane click responses: Implications for cochlear mechanics, *The Journal of the Acoustical Society of America* 110 (1) (2001) 332–348. [doi:10.1121/1.1378349](https://doi.org/10.1121/1.1378349).
- [38] W. Dong, E. S. Olson, Detection of Cochlear Amplification and Its Activation, *Biophysical Journal* 105 (4) (2013) 1067–1078. [doi:10.1016/j.bpj.2013.06.049](https://doi.org/10.1016/j.bpj.2013.06.049).
- [39] S. W. F. Meenderink, W. Dong, Organ of Corti vibrations are dominated by longitudinal motion in vivo, *Communications Biology* 5 (2022) 1285. [doi:10.1038/s42003-022-04234-7](https://doi.org/10.1038/s42003-022-04234-7).

